Journal of Colloid and Interface Science 553 (2019) 269–279

Contents lists available at ScienceDirect

Journal of Colloid and Interface Science

journal homepage: www.elsevier.com/locate/jcis

Regular Article

Guanosine-based thermotropic liquid crystals with tunable phase structures and ion-responsive properties

Zhaohui Huang, Xueyuan Li, Mengjun Chen, Yihan Liu, Xiuping Sun, Aixin Song *, Jingcheng Hao

Key Laboratory of Colloid and Interface Chemistry & Key Laboratory of Special Aggregated Materials, Shandong University, Ministry of Education, Jinan, Shandong Province 250100, China

GRAPHICAL ABSTRACT

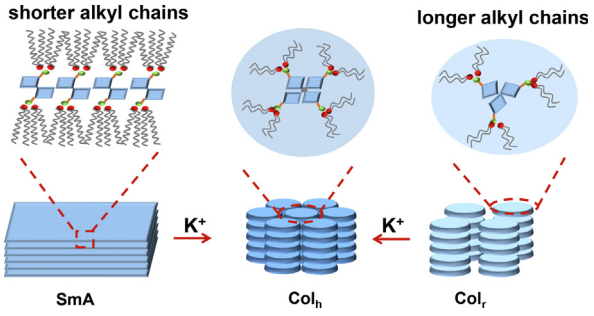

ARTICLE INFO

Article history:
Received 20 February 2019
Revised 11 June 2019
Accepted 12 June 2019
Available online 13 June 2019

Keywords:
Guanosine
Surfactant
Thermotropic liquid crystals
Self-assembly
Stimuli-responsive

ABSTRACT

In this work, the thermotropic liquid crystals (LCs) composed of a biological molecule, guanosine 5′-monophosphate disodium salt (GMP), with different cationic surfactants were reported. When GMP interacted with the surfactants, the length of the surfactant alkyl chains was found to be of great importance in modulating the LC phase. The smectic A (SmA) phase and columnar rectangular (Col_r) phase were formed upon increasing the length of the aliphatic chains due to the enlargement of the steric hindrance. Interestingly, K^+ ions were observed to cause the phase transition of LCs from the SmA or Col_r mesophase to a columnar hexagonal (Col_h) mesophase in the GMP-surfactant complexes, which was attributed to the formation of G-quadruplexes. Accordingly, the chirality and fluorescence properties of the complexes also exhibited K^+-responsive characters as the phase transition of the LCs emerged. Compared with the reported LCs containing guanosine groups, the thermotropic LCs with high elasticity and tunable mesophase structures in this study are easy to be prepared and are hopeful to provide potential applications for constructing stimuli-responsive luminescent materials, biocatalysis and biosensor devices.

1. Introduction

As a class of solvent-free soft materials, thermotropic liquid crystals (LCs) with ordered nanostructures have attracted extensive attention for their versatile functions in developing photoelectric [1], ionic conductive [2], fluorescent materials [3] and sensor devices [4]. Various molecules and compounds have been selected to construct thermotropic LCs driven by different intermolecular interactions such as hydrogen bonding, π-π stacking, van der Waals' force and metal coordination, resulting in nematic, smectic, columnar, and even 3D cubic phases [5–8]. Among these basic building blocks, the molecules with stimuli-responsive properties are very popular to prepare smart LC materials which can exhibit different mesophases under specific conditions [9–11]. Generally,

* Corresponding author.
E-mail address: songaixin@sdu.edu.cn (A. Song).

https://doi.org/10.1016/j.jcis.2019.06.041
0021-9797/

these factors influencing the LC mesophases can be divided into two aspects. On the one hand, as the fundamental structures of the LC molecules always comprise a rigid aromatic core surrounded by several aliphatic chains, the size of the aromatic core [12], the number and the length of the aliphatic chains [13,14] all play significant roles in tuning the LC mesophases, which can be classified as internal effects. On the other hand, when some stimuli-responsive groups are integrate to the building blocks, the resulted LCs tend to transform from one phase to another phase (e.g., from nematic phase to smectic phase) under the stimulus of light [15], electric-field [16], pressure [17] or metal ions [18], which are considered as external effects. More importantly, the transition of the mesophases can make a great difference in modulating the physical and chemical properties of the LCs, including viscoelasticity, conductivity, chirality and the color and intensity of fluorescence [19,20].

Guanosine (G) and its derivatives have both hydrogen bond donors and receptors on their purine rings, which enables them to self-assemble to form ordered structures and be designed for preparing functional materials [21–23]. At the absence of metal ions, guanosine-related molecules are inclined to form ribbon-like architectures (G-ribbons). When certain metals ions, especially K^+ or Sr^{2+} ions, are introduced, the tetrameric arrangements of G-based molecules, G-quartets, tend to be generated driven by ion–dipole interactions, giving rise to G-quadruplex structures through the π-π stacking of G-quartets [24,25]. These versatile G-quadruplex systems provided potential applications in chiral templates [26], metal ion extractants [27], electron transfer [28] and drug design areas [29] in the form of solutions or gels. Davis et al. [30,31] reported the G-quadruplex-based hydrogels stabilized by monovalent metal ions. In our previous work [32], the hydrogels stabilized by trivalent metal ions was first constructed as a response system to pH. The well-ordered lyotropic LCs based on G-specieses were found in water and some organic solvents under appropriate conditions [33,34]. Typically, chiral columnar structures are easy to be observed for the guanine lyotropic mesophases, where the adjacent G-quartets rotate and stack with each other stabilized by non-covalent interactions such as π-π stacking, hydrophilic and hydrophobic interactions [35]. Comparatively, the thermotropic LCs which are also defined as solvent-free LCs formed by G-based molecules have been rarely reported up to now [36]. A series of guanine-oligothiophene conjugates containing different number of hydrocarbon chains were synthesized to investigate their thermotropic LC behaviors [37]. In those work, the hydrocarbon chains were connected to the purine rings through covalent interaction, which needed multi-step, complicated and time-consuming synthesis. As we know, the traditional surfactant molecules always have numerous long aliphatic chains, which have unmatched self-assembly abilities and can aggregate into various nanostructures including micelles [38], vesicles [39], lamellar phase [40] and nanofibers [41], etc. In particular, cationic surfactants can interact with DNA through electrostatic interaction to result in DNA-surfactant complexes, whose self-assembly behaviors have been extensively studied in organic media. The effects of the type of surfactants, DNA and solvents, as well as the charge ratio of surfactant to DNA on the assembled structures have been discussed [42–44]. Recently, some appropriate surfactants have been used as soft part to build supramolecular thermotropic LCs with specific functional molecules like DNA [45], polypeptides [46], polyelectrolytes [47] and even nanoparticles [48]. These complexes are able to form ordered structures in the absence of solvents without changing their intrinsic properties. In this case, similar to DNA, guanosine derivatives with ion-responsive properties can be combined with surfactants through non-covalent interactions to construct intelligent thermotropic LCs.

Herein, we chose a natural guanosine derivative, guanosine 5′-monophosphate disodium salt (abbreviated as GMP), to interact with cationic surfactants through electrostatic interaction. The formation process of the GMP-surfactant complexes was shown in Scheme 1 and the thermotropic LC behaviors of these complexes were observed for the first time. Four surfactants with different alkyl chains, didodecyldimethylammonium bromide (diC_{12}DMAB), dimethylditetradecylammonium bromide (diC_{14}DMAB), dihexadecyldimethylammonium bromide (diC_{16}DMAB) and dimethyldioctadecylammonium bromide (diC_{18}DMAB), were employed to prepare the GMP-surfactant mesophases. All the complexes showed LC phases in a wide range of temperature and the structural transition of the mesophases could be modulated by changing the surfactant alkyl chains. The smectic A (SmA) and columnar rectangular (Col_r) mesophases were produced according to the

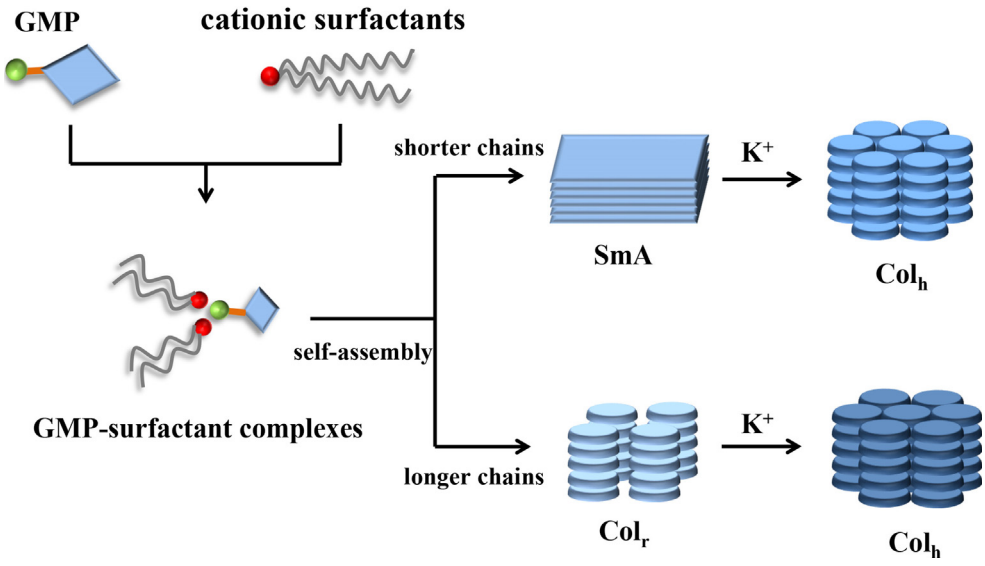

Scheme 1. Schematic diagram of the GMP-surfactant complexes. The SmA phase was self-assembled by the GMP-surfactant complexes with shorter chains while the Col_r phase was self-assembled by the GMP-surfactant complexes with longer chains; the addition of the K^+ induced the transformation of both the SmA phase and Col_r phase to Col_h phase.

length change of alkyl chains. On account of the formation mechanism of the G-quadruplexes, K^+ ions exhibited distinct influence on the transition of the mesophases, inducing the transformation from both the SmA and Col_r phases to a columnar hexagonal (Col_h) phase driven by ion-dipole interaction and π-π stacking. Correspondingly, the chirality and fluorescence of the LCs were successfully tuned accompanied with the phase transition.

2. Experimental section

2.1. Chemicals

Guanosine 5′-monophosphate disodium salt (GMP, 99%), didodecyldimethylammonium bromide (diC_{12}DMAB, 99%), dimethylditetradecylammonium bromide (diC_{14}DMAB, 99%), dihexadecyldimethylammonium bromide (diC_{16}DMAB, 99%), dimethyldioctadecylammonium bromide (diC_{18}DMAB, 99%), and KCl (99%) were purchased from J&K Scientific Ltd. and were used without further purification. The solvents such as chloroform, methanol and ethyl alcohol with analytical grade were provided by Sinopharm Chemical Reagent Co. (China). Water used in the experiments was obtained from a UPH-IV ultrapure water purifier with a resistivity of 18.25 MΩ cm.

2.2. Preparation of GMP-surfactant complexes

All the GMP-surfactant complexes were prepared by precipitation method. Typically, an aqueous solution of 2.00 eq. of the desired surfactant (diC_{12}DMAB, diC_{14}DMAB, diC_{16}DMAB, and diC_{18}DMAB) was added to an aqueous solution of 1.00 eq. GMP (T = 85 °C). The mixtures were stirred for 30 min at 85 °C. After cooling to room temperature, the insoluble complexes were separated from the solution by centrifugation and then washed with ultrapure water for three times. Finally, the complexes were dried in a vacuum oven at 65 °C for 48 h. To make the assemblies more orderly, the dry complexes were dissolved in chloroform again. The resulted chloroform solution was equilibrated at 25.0 ± 0.5 °C for 3 h and then the solvent was gradually evaporated at 50 °C. Then the concentrated solution was dried in a vacuum oven at 60 °C for 24 h to obtain yellow products.

2.3. Preparation of GMP-surfactant-K^+ complexes

KCl was dried under vacuum at 60 °C for at least 12 h before use. The GMP-surfactant-K^+ complexes were prepared by adding the methanol solution of KCl of 4.00 eq. (4.00 mL) to the chloroform solution of the desired GMP-surfactant complexes (GMP-diC_{12}DMAB, GMP-diC_{14}DMAB, GMP-diC_{16}DMAB, and GMP-diC_{18}DMAB) of 1.00 eq. (6.00 mL). The mixtures were stirred at 25 °C for 3 h and then the solvents were slowly removed at 50 °C. The obtained samples were dried under vacuum at 60 °C for 24 h before study.

2.4. Measurements and characterizations

Fourier transform infrared (FTIR) spectra were carried out on a VERTEX-70/70v FT-IR spectrometer (Bruker Optics, Germany). ^1H NMR and ^{31}P NMR spectra were recorded by a Bruker Avance 400-NMR spectrometer operating at 400 MHz. Deuterochloroform (99.8%) was used to prepare the stock solutions. Thermogravimetric analysis (TGA) measurements were performed at DSC 822e (Piscataway, NJ) with a scanning speed of 10 °C·min^{-1} over 30–600 °C under nitrogen atmosphere. Differential scanning calorimetry (DSC) results were obtained by a Q 2000 DSC (New Castle, USA). Samples were heated in aluminum pans under nitrogen flow with an empty aluminum pan using as the reference. The samples were heated at 5 °C·min^{-1}. Polarizing optical microscope (POM) observations were performed on a Motic B2 POM with a hot stage. The samples were first heated to isotropic liquid state and the polarizing optical microscope images were captured in the cooling process (1 °C·min^{-1}).

2.5. Small and wide angle X-ray scattering (SAXS, WAXS) tests

SAXS and WAXS patterns were recorded at SAXSess mc2 (Anton Paar, Austria) with an instrument voltage of 50 kV and an electric current of 40 mA. The incident X-ray wavelength used in this study was 0.154 nm (Cu Kα). The distance from the sample to the detector was 1120 mm. The data accumulation time of each sample was 900 s at 80 °C.

2.6. Rheological experiments

The rheological properties were measured on a Haake RheoStress 6000 rheometer equipped with a cone-plate sensor (C35/1° Ti L07116, diameter: 35 mm, core angle: 1°). The constant temperature was controlled by HAAKE DC10 cyclic water bath (Karlsruhe, Germany). Stress sweep measurements were performed first to measure the mechanical strength and the linear viscoelastic region of the LCs. Then an appropriate stress was chosen from the obtained linear viscoelastic region to carry out the frequency sweep in the range of 0.01–100 Hz.

2.7. Circular dichroism (CD) characterizations

CD spectra were recorded on a Bio-Logic 2,400,304 spectropolarimeter (France) with a scan range of 200–600 nm. The GMP-surfactant and GMP-surfactant-K^+ complexes were dissolved in the mixed solvent of chloroform and methanol (3/2, v/v), respectively (10 mL, 2.50 mM). Each solution was measured at a scanning speed of 100 nm·min^{-1} and repeated 3 times for final curves.

2.8. Fluorescence spectra measurements

The fluorescence spectra were measured on a Hitachi F-7000 fluorescence spectrophotometer with a monochromated Xe lamp as an excitation source. The excitation wavelength used in the experiments was 365 nm. The emission data were recorded from 375 nm to 600 nm with a scan rate of 1200 nm·min^{-1}.

2.9. Materials Studio (MS) calculation

The length of surfactant alkyl chains was calculated by MS. Taking diC_{12}DMAB as an example, the 3D molecule model of diC_{12}-DMAB was drawn by Sketch toolbar of Visualizer block. After the establishment of the molecular structure model, DMol3 block was employed to carry out configuration optimization of the molecule. In detail, the task of "Geometry optimization" was chosen and the "Functional" was set as "LDA" and "PWC". The charge was set to 1. Particularly, the "Quality" was selected as "Medium" with the energy < 2.0e^{-5} Ha, "Max. force" < 0.004 Ha/Å and "Max. displacement" < 0.005 Å. The value of "Max. iterations" was 200. Finally, click the "Run" button. The alkyl chain length of the surfactants was measured by the command of "Distance".

3. Results and discussion

3.1. Preparation and characterization of the complexes

Solvent-free GMP-surfactant complexes were prepared by GMP and cationic surfactants through electrostatic attraction. The

chemical structures of GMP and different cationic surfactants are shown in Fig. 1a and b. The interactions between GMP and surfactants were detected by FTIR, ^{1}H NMR and ^{31}P NMR. As shown in Fig. 1c, the characteristic absorption bands with strong intensity at 2800–3000 cm^{-1} of —CH_2— and —CH_3 were present for the GMP-surfactant complexes, indicating the existence of the aliphatic chains of the surfactants. The absorption band at 1084 cm^{-1} of GMP corresponds to the symmetric stretching vibration of non-esterified P—O bonds [49,50]. When GMP interacts with the cationic surfactants, the electrostatic interaction disturbs this vibration, leading to the lower absorption intensity. The spectra of all the complexes appear a broad peak at around 2700–3700 cm^{-1}, confirming the formation of hydrogen bonding between the guanine skeletons of GMP [37]. The ^{1}H NMR spectra of the four complexes (GMP-diC_{12}DMAB, GMP-diC_{14}DMAB, GMP-diC_{16}DMAB and GMP-diC_{18}DMAB) are shown in Fig. 1d and e. The ^{1}H NMR signals of the surfactants and GMP are assigned as *a* to *f* and *a′* to *f′*, respectively [51–53], demonstrating the successful combination of the cationic surfactants with GMP. It is worth noting that there are some differences between the spectra of GMP-diC_{12}DMAB and the other three complexes. As can be seen from Fig. 1e, the proton signal peaks of GMP-diC_{12}DMAB are smooth and broad while those of the other three complexes are rather sharp. It is speculated that the difference may be ascribed to the different molecular arrangements of the complexes. The ^{31}P NMR spectra (Fig. S1) show only one phosphorus signal for each complex, indicating a single phosphorus environment and demonstrating that the four complexes prepared are of rather high purity.

3.2. Properties of liquid crystals

The mesophase textures of the four thermotropic LCs were observed on a polarising optical microscope (POM) with a hot stage. As shown in Fig. 2a, the GMP-diC_{12}DMAB complex exhibited the typical focal-conic texture of smectic layers when being cooled from the isotropic liquid state [45,46]. The small-angle X-ray

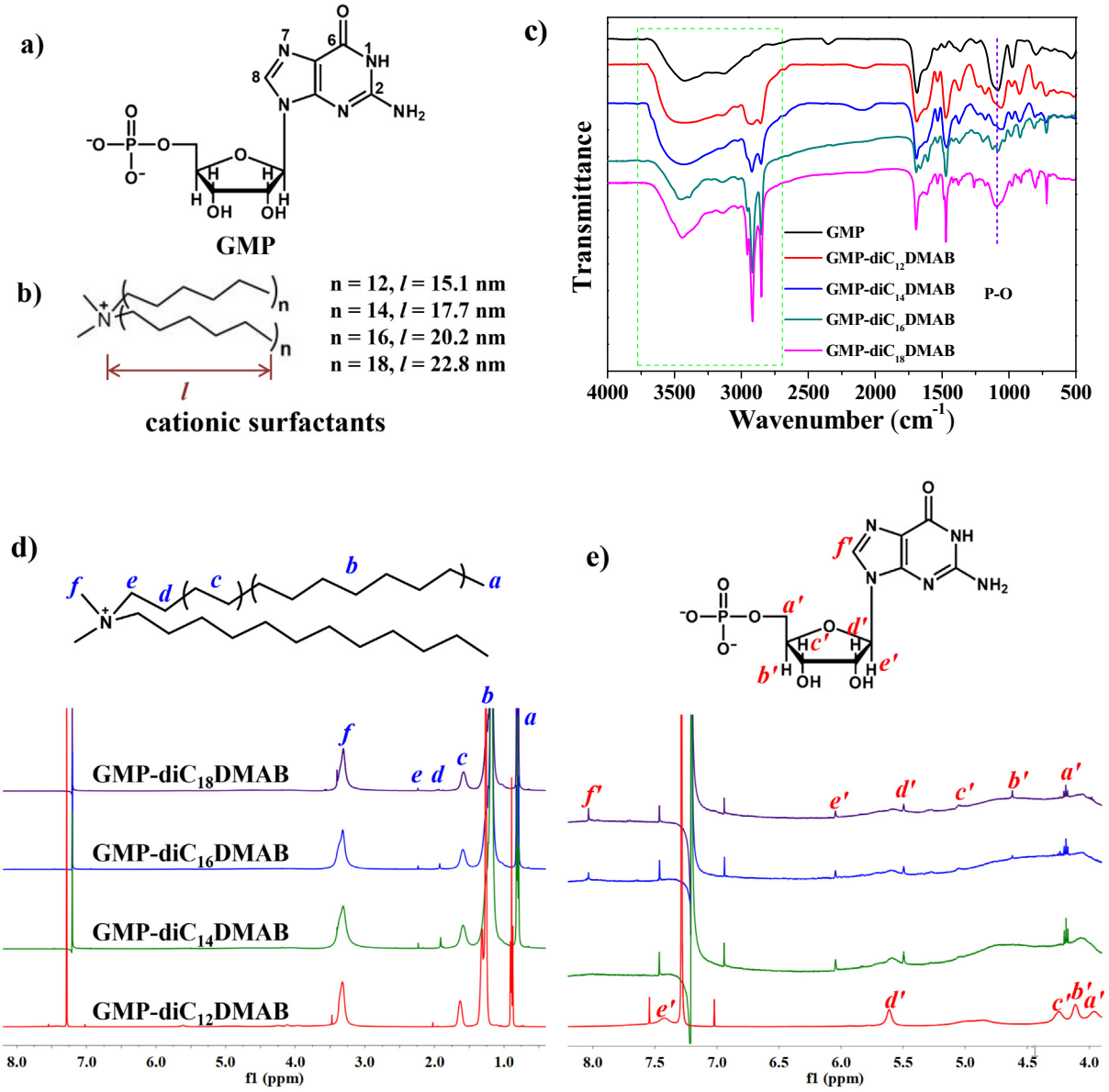

Fig. 1. (a) The chemical structure of GMP; (b) The four cationic surfactants and their corresponding alkyl chain length measured by Materials Studio; (c) FTIR spectra of GMP and four GMP-surfactant complexes; (d) ^{1}H NMR spectra and proton assignments of the surfactants in GMP-surfactant complexes; (e) the enlarged region of d in 8.2–3.2 ppm. The proton signals are assigned to the GMP in GMP-surfactant complexes. The solvent is $CDCl_3$.

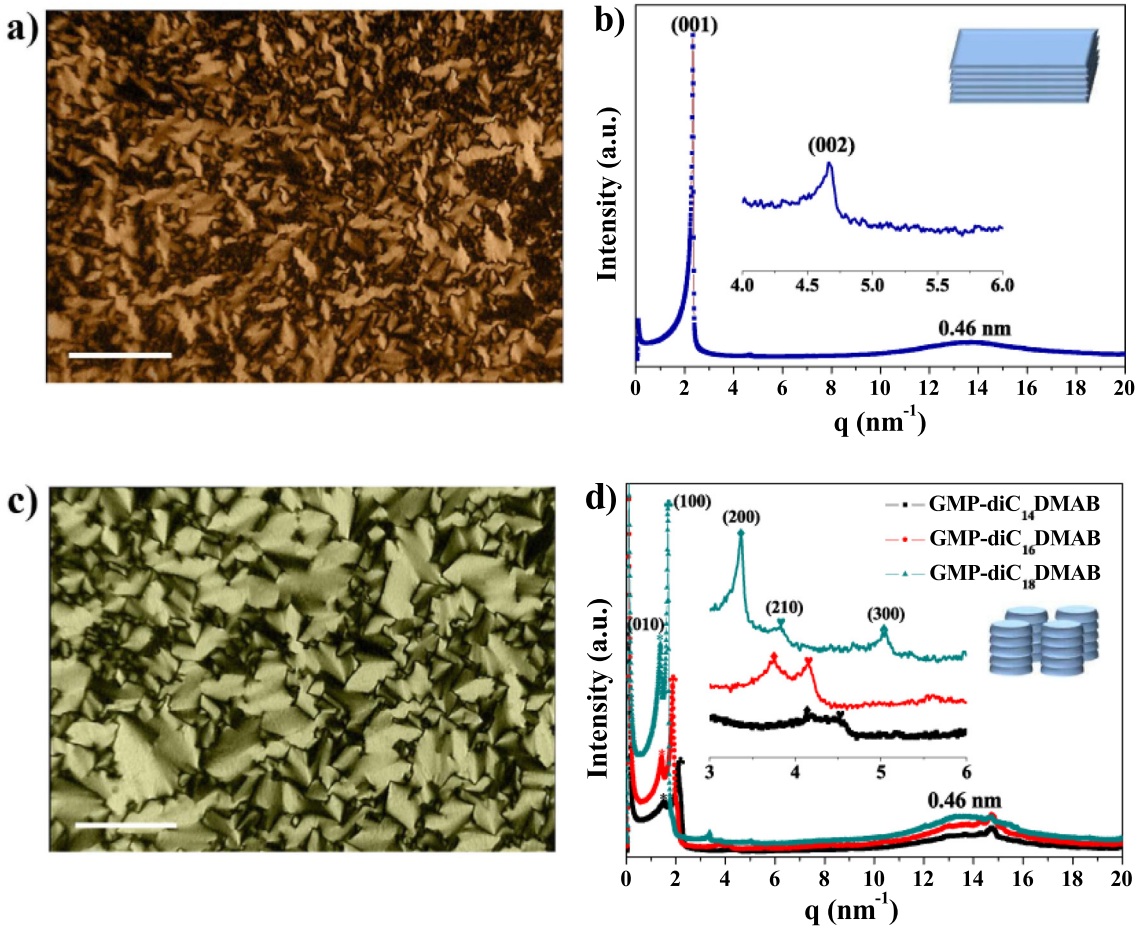

Fig. 2. (a) The POM image and (b) SAXS pattern of GMP-diC$_{12}$DMAB complexes at 80 °C; (c) POM image of GMP-diC$_{18}$DMAB complexes at 80 °C; (d) SAXS pattern of GMP-diC$_{14}$DMAB, GMP-diC$_{16}$DMAB and GMP-diC$_{18}$DMAB complexes in the Col$_r$ LC phase at 80 °C. All the POM images were captured during cooling process from their isotropic phases. Scale bar, 100 μm.

scattering (SAXS) pattern of the LC composed of GMP-diC$_{12}$DMAB complex (Fig. 2b) at 80 °C displayed two small-angle Bragg reflections in a 1:2 ratio, indicating the (0 0 1) and (0 0 2) planes of SmA LC phase [54]. The first sharp reflection at q = 2.33 nm^{-1} is corresponding to the layer spacing of 26.9 Å ($d = 2\pi/q$) of the well-defined lamellar structure (Table 1). The thickness of the guanosine layer is about 10.0 Å and the surfactant bilayer with fully extended aliphatic chains is ~ 30.2 Å measured by Materials Studio (MS). Compared with the layer spacing obtained from SAXS (~26.9 Å) and the results calculated by MS (~31.2 Å), we can draw the conclusion that the neighboring alkyl chains of the surfactant tend to interdigitate with each other in LC state. At wide angle region, a broad scattering halo at around 13.6 nm^{-1} indicated the typical distance of 4.60 Å between the flexible molten alkyl chains of the complexes (short-range alignment), which reflected the fluid-like properties of the LCs [55].

Considering the elongation of hydrocarbon chains was prone to make a difference to the self-assembly behaviors, we studied the LC phases composed of GMP and the surfactants with longer aliphatic chains [14]. The broken fan-shaped textures, which were commonly generated from columnar mesophases [56], were observed from the POM images of GMP-diC$_{14}$DMAB, GMP-diC$_{16}$DMAB and GMP-diC$_{18}$DMAB complexes at the cooling process (Fig. S2a, S2b and Fig. 2c). The SAXS profiles of the three complexes at 80 °C exhibited that the first-order reflection split into two peaks which were rather close to each other (Fig. 2d), suggesting the presence of a Col$_r$ mesophase [56]. The Bragg peaks of each complex displayed at small-angle regions could be indexed as (0 1 0), (1 0 0), (2 0 0) and (2 1 0) planes of a Col$_r$ phase with p2mm symmetry, of which the lattice parameters [57] were listed in Table 1. At the wide angle region, a diffuse halo (4.60 Å) with several reflections between 13.6 and 14.8 nm^{-1} was also observed for each Col$_r$ mesophase, confirming the ordered packing of the molten hydrocarbon chains (Fig. 2d). The correlation between the surfactant chain length and the layer spacing (the maximum distance between two adjacent columns) of the Col$_r$ LCs was summarized in Table 1. When the length of the alkyl chains increases, one can find the q value of the first reflection decreases from 1.53 nm^{-1} to 1.38 nm^{-1}, indicating that the layer spacing increases from 41.0 Å to 45.6 Å. The number of molecules in one unit cell (Z) can be calculated based on Eq. (1) [58],

$$Z = \frac{\rho \cdot NA \cdot A \cdot h}{Mr} \quad (1)$$

where ρ is the density of the LC phase (assuming ρ = 1 g·cm^{-3} for organic molecules in this study), N_A is the Avogadro's constant, A represents the columnar cross area which can be estimated by lattice parameters ($a \times b$), h is the height of the columnar slice (the d-spacing calculated by the hole in the wide-angle region of SAXS profile) and M_r stands for the weight of a complex molecule. Herein, the Z values of the three Col$_r$ mesophases were calculated all to be 3, manifesting that there were three GMP-surfactant complex molecules self-assembled into a discoid unit, and these discoid units further stacked to form the rectangular columnar structures.

Table 1
Structural parameters of GMP-surfactant mesophases.

	Mesophase	Lattice parameters (Å)	Layer spacings (Å)	Miller indices	Z	T (°C)
GMP-diC$_{12}$DMAB	SmA	–	26.9	001	–	80
			13.4	002		
			4.6	halo		
GMP-diC$_{14}$DMAB	Col$_r$	a = 29.9	41.0	010	3	80
	p2mm	b = 41.0	29.9	100		
			15.2	200		
			14.1	210		
			4.6	halo		
GMP-diC$_{16}$DMAB	Col$_r$	a = 33.5	43.8	010	3	80
	p2mm	b = 43.8	33.5	100		
			16.7	200		
			15.1	210		
			4.5	halo		
GMP-diC$_{18}$DMAB	Col$_r$	a = 37.3	45.6	010	3	80
	p2mm	b = 45.6	37.3	100		
			18.7	200		
			16.4	210		
			12.4	300		
			4.6	halo		

3.3. Thermotropic properties of the LCs

Thermogravimetric analysis (TGA) was performed to explore the thermostability of the GMP-surfactant mesophases. As shown in Fig. S3 and Table S1, both the SmA and Col$_r$ samples have good thermal stability with the decomposition temperature (T$_d$) over 200 °C. It is noticed that T$_d$ of the complexes increases from 201 °C to 215 °C with the increase in carbon number from 12 to 18. The similar correlation can also be observed between the phase transition temperatures and the length of the surfactant alkyl chains. As summarized from the differential scanning calorimetry (DSC) curves (Fig. S4), the melting and clearing points of the complexes rise generally with the increasing aliphatic chain length (Fig. 3). We speculate that the increases in the decomposition and phase transition temperatures both result from the stronger van der Waals' interaction between the longer aliphatic chains of the surfactants [55]. Some obvious differences between the lamellar mesophase and the other three Col$_r$ mesophases were observed when examined by DSC. For the SmA phase assembled from GMP-diC$_{12}$DMAB complex, no glass transition temperature (T_g) appeared both in the heating and cooling process, and only the crystal state was generated due to the crystallization of the densely ordered packing of surfactant alkyl chains, which could be kept even at very low temperature. However, for the Col$_r$ LCs built by GMP with the surfactants with longer alkyl tails, T_g was present below the crystallization temperature (T_c). The phase transition of the Col$_r$ samples from the crystal state to glassy state was perhaps because the ordered packing of the alkyl chains was not as dense as that of SmA samples. When temperature gradually decreased, the alkyl chains of the Col$_r$ samples could not move randomly, and as a result, the ordered arrangements of the alkyl chains were destroyed to form a relatively disordered structure [59]. It should be noted that the clearing point of the Col$_r$ mesophase from GMP-diC$_{18}$DMAB complex was not detected by DSC even though the mesophase was heated to around T_d (215 °C). In this case, we consider that its clearing point may be higher than T_d at the atmospheric pressure.

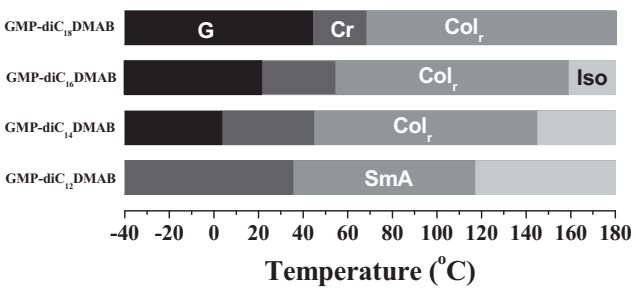

Fig. 3. The phase region of the GMP-surfactant complexes. G, glassy state; Cr, crystal; SmA, smectic A phase; Col$_r$, columnar rectangular phase; Iso, isotropic liquid.

3.4. Rheological properties

Rheological measurements were carried out to estimate the viscoelastic properties of the GMP-surfactant mesophases. The storage modulus (G') and the yield stress (τ_y) can be obtained from the stress sweep results, which are generally employed to evaluate the mechanical strength of samples. The value of τ_y is corresponding to the critical shear stress when the plateau value of G' decreases sharply [40]. As shown in Fig. 4a, the mechanical strength of the LC samples with different microstructures exhibits a dependence on the alkyl chain length at 80 °C, where both the values of τ_y (from ~199 to ~2512 Pa) and G' (from ~10^4 to ~10^6 Pa) gradually increased with the increasing alkyl chain length. We can conclude that the mechanical strength of the thermotropic LCs can be tuned by changing the alkyl chain length. Herrmann et al. reported the thermotropic LCs composed of DNA and double long-chained cationic surfactants [60]. In their study, the thermotropic LCs exhibited fluidic property. In the present study, the thermotropic LCs were constructed by GMP, one of the basic building blocks of DNA, and double-chained cationic surfactants. From Figs. 4b–d and S5, one can find that the value of G' is about an order magnitude higher than that of G'' at 80 °C both for the smectic and columnar thermotropic LCs, indicating the solid-like behavior rather than fluidic property. We speculate that this difference may be attributed to the stronger van der Waals force among the longer alkyl chains in this study than that of the shorter alkyl chains in DNA-based thermotropic LC systems. In addition, the differences in electrostatic interaction and hydrogen bonding can also lead to the different physical states of the thermotropic LCs.

3.5. K^+-induced phase transition of the LCs

Guanosine derivatives are preferential to form G-quadruplexes in the presence of certain metal ions (usually some alkali metal

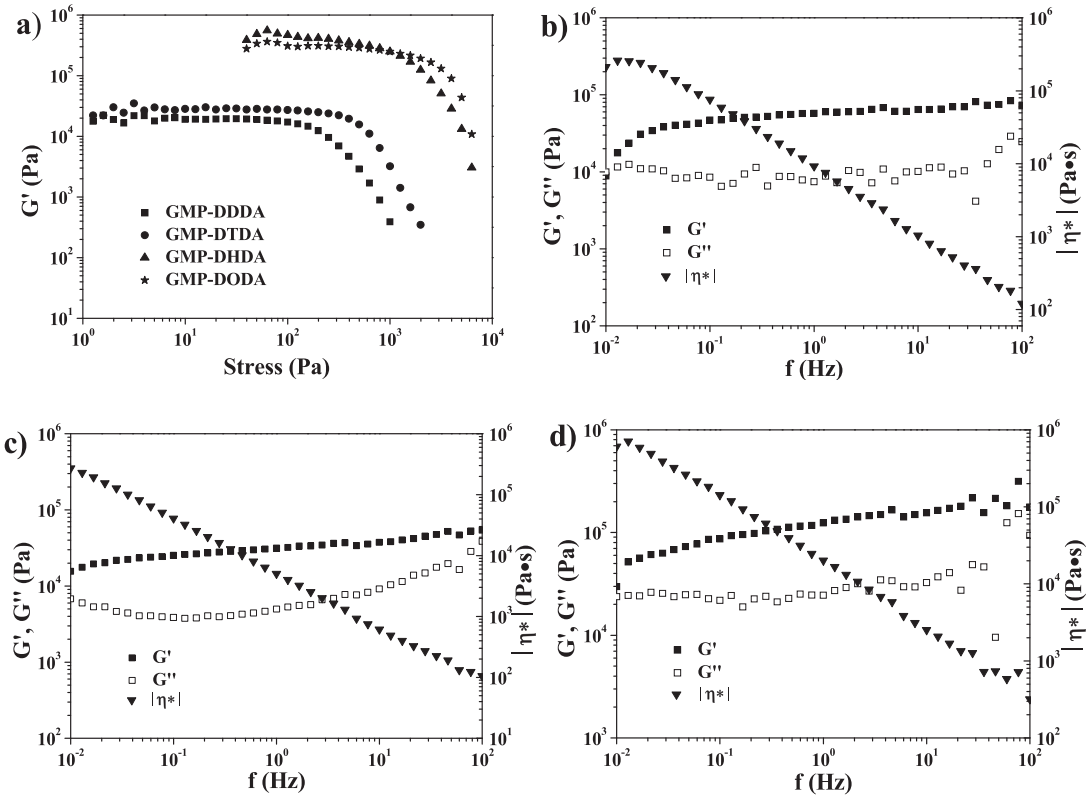

Fig. 4. (a) Stress sweep results of the GMP-surfactant mesophases with different surfactant alkyl chains at 80 °C; frequency sweep results of (b) GMP-diC_{12}DMAB, (c) GMP-diC_{14}DMAB and (d) GMP-diC_{16}DMAB complexes at 80 °C.

ions). In this work, K^+ ions were introduced into the GMP-surfactant complexes to detect the phase structural transition induced by the G-quartets or G-quadruplexes. Herein, the GMP-diC_{12}DMAB complex (SmA mesophase) and GMP-diC_{14}DMAB complex (Col_r mesophase) were chosen to interact with K^+ ions. As shown in FTIR spectra (Fig. S6a), the absorption signal at 1688 cm^{-1} of GMP assigned to C═O shifted to a higher wavenumber in the presence of K^+ ions (1692 cm^{-1} for GMP-diC_{12}DMAB-K^+ and 1694 cm^{-1} for GMP-diC_{14}DMAB-K^+). This change can be ascribed to the ion-dipole interaction between K^+ ions and the guanine groups [32]. POM, SAXS and WAXS were applied to investigate the influence of K^+ ions on the microstructures. As shown in Fig. 5a, the POM image of the GMP-diC_{12}DMAB-K^+ complex showed fan-shaped textures when being cooled from the isotropic liquid state, where the SAXS pattern at 80 °C exhibited two Bragg reflections which could be indexed as (1 0 0) and (1 1 0) with the q ratio of $1:\sqrt{3}$ (Fig. 5b). This result confirmed the transformation of GMP-diC_{12}DMAB complex from SmA mesophase to Col_h mesophase under the addition of K^+ ions [61]. For GMP-diC_{14}DMAB-K^+ complex, the SAXS profile was similar to that of GMP-diC_{12}DMAB-K^+ complex with similar fan-shaped textures also observed in POM image(Fig. 5c and d), indicating that the introduction of K^+ ions led to a phase transformation from the Col_r phase to Col_h phase. The relevant lattice parameters and layer spacing of the two Col_h mesophases were listed in Table 2. Notably, the value of Z was calculated to be 4, implying that four complex molecules self-assembled into disk-like aggregates, which further organized into the Col_h structures. Furthermore, the d values of 3.36 Å (GMP-diC_{12}DMAB-K^+ complex) and 3.38 Å (GMP-diC_{14}DMAB-K^+ complex) were the typical distance between two adjacent G-quartets, confirming the formation of G-quadruplexes induced by K^+ ions [21]. The DSC analysis showed that the complexes containing K^+ ions could keep Col_h phase in a wide temperature range, and their phase transition temperature increased with the elongation of the surfactant aliphatic chains (Fig. S6b and c).

3.6. Phase transition mechanisms of the LCs

It is commonly considered that the self-assembly behavior of molecules is closely related to their size and shape [62]. Based on this understanding, we discussed the possible mechanisms how the alkyl chain length of surfactants affected the LCs phase. As displayed in Fig. 6, the guanosine groups are inclined to self-assemble into ribbon-like architectures driven by hydrogen bonding in the absence of metal ions as templates. When the length of the alkyl chains is short, there is enough space for alkyl chains to arrange on both sides of the G-ribbon structures to form a SmA phase with lamellar structure through the strong van der Waals' force. Each repeating layer is composed of numerous tail-to-tail interacting cationic surfactants which are attached to GMP anions driven by electrostatic interactions. Upon increasing the length of the aliphatic chains, the generated larger steric hindrance is unfavorable to the formation of lamellar structures. In this case, three complex molecules self-assemble into the G-triplets structures, resulting in irregular disk-like units which further aggregate to a Col_r phase driven by π-π stacking. In addition, it has been reported that the volume fraction of the alkyl chains (f_R) in a LC molecule could be used to derermin the LC mesophase [14]. In this study, the volumes of surfactant alkyl chains (V_R) and GMP (V_{GMP}) were calculated using the crystal volume increments and listed in Table 3 [63]. The values of f_R were obtained correspondingly and shown in Table 3. It is obvious that the value of f_R increases with increasing the surfactant alkyl chain length. As we can seen, the SmA phase is formed when $f_R = 0.64$, while the Col_r phase is generated when $f_R > 0.64$. It is concluded that the value of f_R which is closely related to the length of surfactant alkyl chains can be used to preliminarily

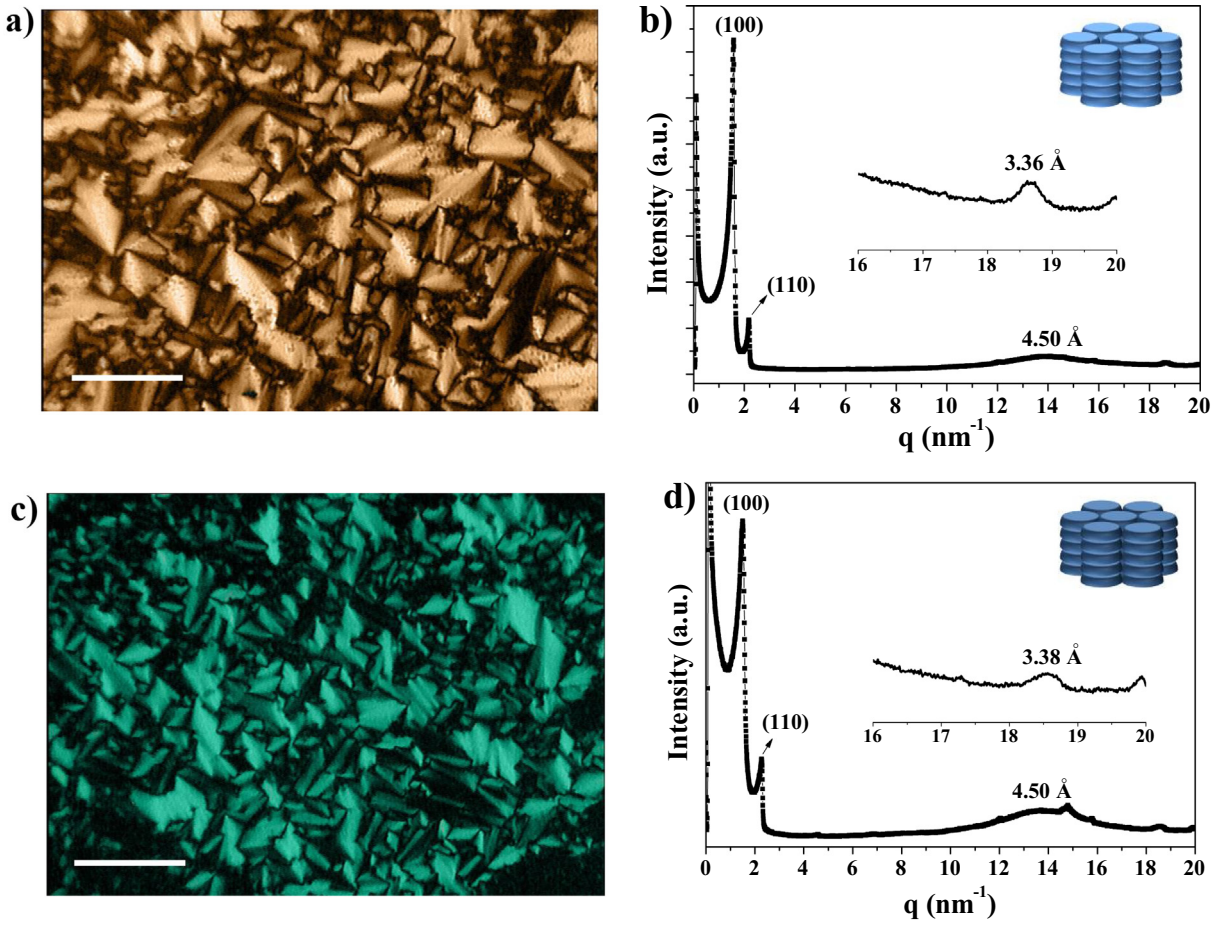

Fig. 5. (a) POM image and (b) SAXS pattern of GMP-diC_{12}DMAB-K^+ complexes at 80 °C; (c) POM image and (d) SAXS pattern of GMP-diC_{14}DMAB-K^+ complexes at 80 °C. All the POM images were captured during cooling process from their isotropic phases. Scale bar, 100 μm.

Table 2
Structural parameters of GMP-surfactant-K^+ mesophases.

	Mesophase	Lattice parameters (Å)	Layer spacings (Å)	Miller indices	Z	T (°C)
GMP-diC_{12}DMAB-K^+	Col_h p6mm	a = 45.9	39.8 28.7 4.6	100 110 halo	4	80
GMP-diC_{14}DMAB-K^+	Col_h p6mm	a = 50.9	44.2 27.6 4.6	100 110 halo	4	80

estimate the type of mesophase of LCs. When K^+ ions are introduced into the SmA or Col_r phase, the strong ion-dipole interaction between K^+ ions and guanine groups induces the generation of G-quartets by four complex molecules, which further stack into the Col_h phase with more symmetry.

3.7. Chiral and fluorescent properties

The phase transition of LCs led to some property changes, such as chirality and fluorescence [19,20]. Herein, we discussed the chiral properties of the GMP-surfactant complexes in the absence and presence of K^+ ions. From CD spectra in Fig. 7a, a peak of the GMP-diC_{12}DMAB-K^+ complex with strong intensity at ~300 nm appeared, while no signal of the GMP-diC_{12}DMAB complex was observed, suggesting the formation of chiral columnar structures along with the transformation from SmA to Col_h phase [64]. For the GMP-diC_{14}DMAB complex, the chiral peak at ~303 nm existed both before and after the addition of K^+ ions. When the phase transition from the Col_r phase to Col_h phase was achieved, the peak intensity enhanced remarkably. We consider that the chirality changes are attributed to the ordered stacking of G-quartets induced by the ion–dipole interaction wherein one K^+ ion effectively interacted with four guanine groups [32].

Fluorescent properties of the complexes were subsequently studied under the illumination at 365 nm (Fig. 7b–g). To quantitatively compare the fluorescence intensity, the solutions of the complexes with a concentration of 2.50 mM in chloroform-methanol mixed solvents (3:2, v/v) were measured under the same condition. From the obtained emission spectra (Fig. 7b), one can find that the intensity enhances when the GMP-diC_{12}DMAB SmA phase transforms to the GMP-diC_{12}DMAB-K^+ Col_h phase, with a bathochromic shift of the absorption peak from 417 nm to 439 nm. This

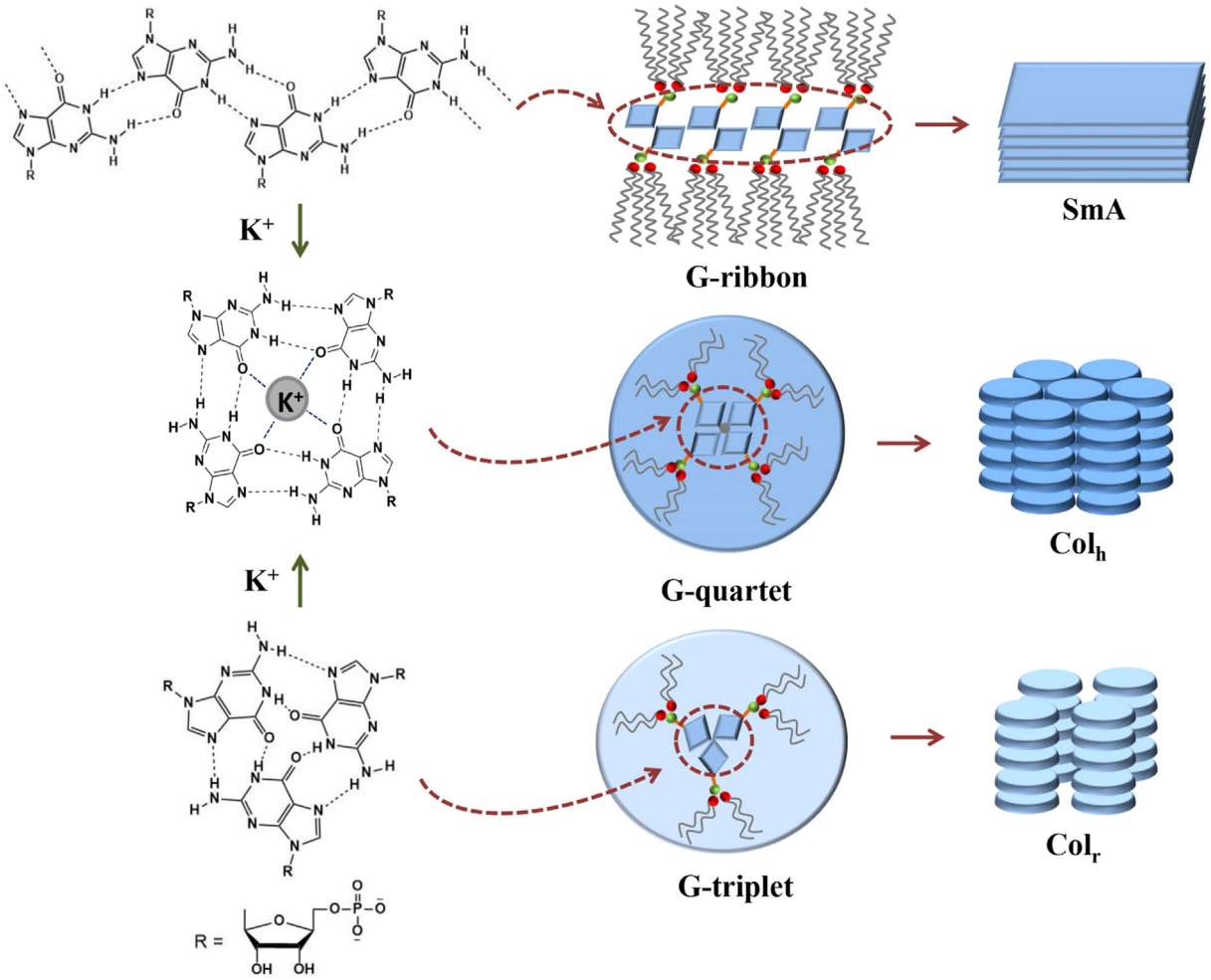

Fig. 6. Schematic diagram of the LCs phase transition induced by the alkyl chains and K^+ ions.

Table 3
Volumes of surfactant alkyl chains (V_R) and GMP (V_{GMP}), and the related volume fractions (f_R) and LC mesophases.

Complex	V_R (Å^3)	V_{GMP} (Å^3)	f_R	Mesophase
GMP-diC_{12}DMAB	616.2	351.8	0.64	SmA
GMP-diC_{14}DMAB	715.4	351.8	0.67	Col_r
GMP-diC_{16}DMAB	814.6	351.8	0.70	Col_r
GMP-diC_{18}DMAB	886.2	351.8	0.72	Col_r

result is consistent with the fluorescent color change from blue to cyan, as shown in Fig. 7c-1 and c-2. Similarly, for GMP-diC_{14}DMAB complex, the fluorescence intensity at 438 nm was also visibly increased when the Col_r phase was converted into the Col_h phase under the introduction of K^+ ions. Several previous studies reported that the different rotational motions of the intercolumnar aromatic rings caused the changes of the fluorescent properties when the Col_r phase transformed to the Col_h phase [65]. In this study, another possible reason might be that the addition of K^+ ions resulted in the formation of more π-π stacking structures with ordered arrangements, which effectively contributed to the enhancement of the fluorescence intensity. The K^+-responsive property of the LCs is consistent with previous reports which have demonstrated that K^+ ions have strong binding ability with guanosine molecules.

4. Conclusions

We have constructed the thermotropic LCs of GMP-surfactant complexes driven by non-covalent interactions such as electrostatic interaction, hydrogen bonding and van der Waals' force. The structure of LCs can be modulated by changing the length of the surfactant chains or introducing K^+ ions into the complexes. For the GMP-diC_{12}DMAB complexes with shorter alkyl chains, the SmA phase was formed; while for the GMP-surfactant complexes with longer alkyl chains, the Col_r phase tended to be generated. In this process, the difference in the steric hindrance induced by surfactants plays an important role in tuning the LC phase structures. The introduction of K^+ ions triggered the phase transition due to the formation of G-quadruplexes, for which the Col_h mesophase was produced instead of the SmA or Col_r mesophase. The guanosine derivatives have been widely studied in formation of gel state [30–32], while the thermotropic LCs based on guanosine were not often observed. Up to now, only several systems of LCs consisting of guanosine derivatives synthesized by covalent method have been reported [20,36,37]. Comparatively, the thermotropic LCs in this work are easily prepared and their phase transition can be realized through changing the surfactant structures, showing the flexible regulation for the construction of LCs with diverse structures and properties. The changes of mechanical strength, chiral and fluorescent properties along with the phase transition are hopeful to make the LCs become promising

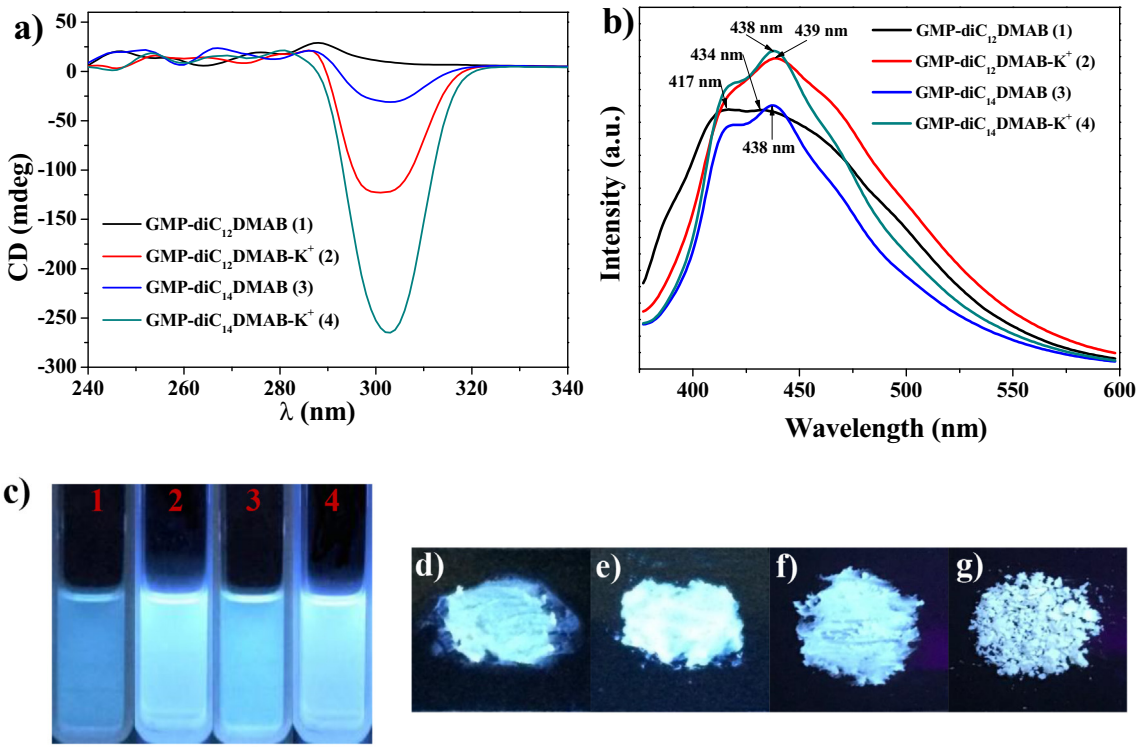

Fig. 7. (a) CD spectra and (b) fluorescence spectra of the mesophases; (c) the fluorescence images of 2.5 mM GMP-surfactant-(K^+) complexes in $CHCl_3$-CH_3OH mixed solvents (3:2, v/v): GMP-diC_{12}DMAB (c-1), GMP-diC_{12}DMAB-K^+ (c-2), GMP-diC_{14}DMAB (c-3) and GMP-diC_{14}DMAB-K^+ (c-4); the fluorescence images of (d) GMP-diC_{12}DMAB, (e) GMP-diC_{12}DMAB-K^+, (f) GMP-diC_{14}DMAB and (g) GMP-diC_{14}DMAB-K^+ complexes in solid state. The excitation wavelength is 365 nm.

candidates for the development of smart materials and biosensor devices.

Acknowledgements

This work was funded by the National Natural Science Foundation of China (Nos. 21573134 and 21420102006).

Appendix A. Supplementary material

Additional images of POM, TGA, DSC, rheology and FTIR are appended in the supporting information. These information are available in the online version of the paper. Supplementary data to this article can be found online at https://doi.org/10.1016/j.jcis.2019.06.041.

References

[1] T.Z. Shen, S.H. Hong, J.H. Lee, S.G. Kang, B. Lee, D. Whang, J.K. Song, Adv. Mater. 30 (2018) 1802441.
[2] J. Sakuda, E. Hosono, M. Yoshio, T. Ichikawa, T. Matsumoto, H. Ohno, H. Zhou, T. Kato, Adv. Funct. Mater. 25 (2015) 1206–1212.
[3] S. Yagai, S. Okamura, Y. Nakano, M. Yamauchi, K. Kishikawa, T. Karatsu, A. Kitamura, A. Ueno, D. Kuzuhara, H. Yamada, T. Seki, H. Ito, Nat. Commun. 5 (2014) 4013–4023.
[4] F. Zuo, Z. Liao, C. Zhao, Z. Qin, X. Li, C. Zhang, D. Liu, Chem. Commun. 50 (2014) 1857–1860.
[5] K. Goossens, K. Lava, C.W. Bielawski, K. Binnemans, Chem. Rev. 116 (2016) 4643–4807.
[6] C. Tschierske, Angew. Chem. Int. Ed. 52 (2013) 8828–8878.
[7] T. Kato, M. Yoshio, T. Ichikawa, B. Soberats, H. Ohno, M. Funahashi, Nat. Rev. Mater. 2 (2017) 17001.
[8] K. Liu, C. Ma, R. Göstl, L. Zhang, A. Herrmann, Acc. Chem. Res. 50 (2017) 1212–1221.
[9] T. Kosa, L. Sukhomlinova, L. Su, B. Taheri, T.J. White, T.J. Bunning, Nature 485 (2012) 347–349.
[10] B. Huitorel, Q. Benito, A. Fargues, A. Garcia, T. Gacoin, J.P. Boilot, S. Perruchas, F. Camerel, Chem. Mater. 28 (2016) 8190–8200.
[11] M.L. Bushey, T.Q. Nguyen, C. Nuckolls, J. Am. Chem. Soc. 125 (2003) 8264–8269.
[12] M. Lehmann, Chem. Eur. J. 15 (2009) 3638–3651.
[13] F. Liu, M. Prehm, X. Zeng, C. Tschierske, G. Ungar, J. Am. Chem. Soc. 136 (2014) 6846–6849.
[14] X. Cheng, F. Su, R. Huang, H. Gao, M. Prehm, C. Tschierske, Soft Matter 8 (2012) 2274–2285.
[15] Y. Kim, N. Tamaoki, ACS Appl. Mater. Interfaces 8 (2016) 4918–4926.
[16] L. Zhang, C. Ma, J. Sun, B. Shao, G. Portale, D. Chen, K. Liu, A. Herrmann, Angew. Chem. Int. Ed. 57 (2018) 6878–6882.
[17] E. Gorecka, D. Pociecha, J. Mieczkowski, J. Matraszek, D. Guillon, B. Donnio, J. Am. Chem. Soc. 126 (2004) 15946–15947.
[18] S. Kohmoto, E. Mori, K. Kishikawa, J. Am. Chem. Soc. 129 (2007) 13364–13365.
[19] Y. Sagara, T. Kato, Nat. Chem. 1 (2009) 605–610.
[20] T. Kato, T. Matsuoka, M. Nishii, Y. Kamikawa, K. Kanie, T. Nishimura, E. Yashima, S. Ujiie, Angew. Chem. Int. Ed. 43 (2004) 1969–1972.
[21] J.T. Davis, G.P. Spada, Chem. Soc. Rev. 36 (2007) 296–313.
[22] S. Lena, S. Masiero, S. Pieraccini, G.P. Spada, Chem. Eur. J. 15 (2009) 7792–7806.
[23] Y. Wu, K.E. Brown, M.R. Wasielewski, J. Am. Chem. Soc. 135 (2013) 13322–13325.
[24] D.G. Rodríguez, P.G.A. Janssen, R.M. Rapún, I. De Cat, S. De Feyter, A.P.H.J. Schenning, E.W. Meijer, J. Am. Chem. Soc. 132 (2010) 4710–4719.
[25] S. Pieraccini, S. Masiero, O. Pandoli, P. Samorì, G.P. Spada, Org. Lett. 8 (2006) 3125–3128.
[26] C.A. Hrault, A. Banu, M. Barboiu, M. Michau, A. van der Lee, Angew. Chem. Int. Ed. 46 (2007) 4268–4272.
[27] F.W.B. van Leeuwen, W. Verboom, X. Shi, J.T. Davis, D.N. Reinhoudt, J. Am. Chem. Soc. 126 (2004) 16575–16581.
[28] Y. Wu, K.E. Brown, D.M. Gardner, S.M. Dyar, M.R. Wasielewski, J. Am. Chem. Soc. 137 (2015) 3981–3990.
[29] E.S. Baker, J.T. Lee, J.L. Sessler, M.T. Bowers, J. Am. Chem. Soc. 128 (2006) 2641–2648.
[30] G.M. Peters, L.P. Skala, T.N. Plank, H. Oh, G.N.M. Reddy, A. Marsh, S.P. Brown, S. R. Raghavan, J.T. Davis, J. Am. Chem. Soc. 137 (2015) 5819–5827.
[31] G.M. Peters, L.P. Skala, J.T. Davis, J. Am. Chem. Soc. 138 (2016) 134–139.
[32] J. Zhang, X. Li, X. Sun, A. Song, Y. Tan, J. Hao, Sci. China Chem. 61 (2018) 604–612.
[33] P. Mariani, C. Mazabard, A. Garbesi, G.P. Spada, J. Am. Chem. Soc. 111 (1989) 6369–6373.
[34] J.P. Mathias, E.E. Simanek, J.A. Zerkowski, C.T. Seto, G.M. Whiteside, J. Am. Chem. Soc. 116 (1994) 4316–4325.
[35] F. Ciuchi, G.D. Nicola, H. Franz, G. Gottarelli, P. Mariani, M.G.P. Bossi, G.P. Spada, J. Am. Chem. Soc. 116 (1994) 7064–7071.
[36] G. Laughlan, A.H. Murchie, D.G. Norman, M.H. Moore, P.C.E. Moody, D.M.J. Lilley, B. Luisi, Science 265 (1994) 520–524.

[37] K.P. Gan, M. Yoshio, Y. Sugihara, T. Kato, Chem. Sci. 9 (2018) 576–585.
[38] D. Wang, Y. Sun, M. Cao, J. Wang, J. Hao, RSC Adv. 5 (2015) 95604–95612.
[39] S. Song, H. Wang, A. Song, S. Dong, J. Hao, Chem. Eur. J. 20 (2014) 9063–9072.
[40] X. Wang, J. Hao, J. Phys. Chem. B 119 (2015) 13321–13329.
[41] Y. Hu, W. Xu, G. Li, L. Xu, A. Song, J. Hao, Langmuir 31 (2015) 8599–8605.
[42] K. Tanaka, Y. Okahata, J. Am. Chem. Soc. 118 (1996) 10679–10683.
[43] X. Hou, M. Xu, L. Wu, J. Shen, Colloids Surf. B 41 (2005) 181–187.
[44] L. Niu, J. Yan, X. Yang, C. Burger, L. Rong, B. Hsiao, D. Liang, Sci. China Chem. 57 (2014) 1738–1745.
[45] K. Liu, J. Varghese, J.Y. Gerasimov, A.O. Polyakov, M. Shuai, J. Su, D. Chen, W. Zajaczkowski, A. Marcozzi, W. Pisula, B. Noheda, T.T.M. Palstra, N.A. Clark, A. Herrmann, Nat. Commun. 7 (2016) 11476–11486.
[46] K. Liu, D. Pesce, C. Ma, M. Tuchband, M. Shuai, D. Chen, J. Su, Q. Liu, J.Y. Gerasimov, A. Kolbe, W. Zajaczkowski, W. Pisula, K. Müllen, N.A. Clark, A. Herrmann, Adv. Mater. 27 (2015) 2459–2465.
[47] M.L. Cortez, M. Ceolín, L.C. Camacho, E. Donath, S.E. Moya, F. Battaglini, O. Azzaroni, ACS Appl. Mater. Interfaces 9 (2017) 1119–1128.
[48] M. Mendozza, C. Montis, L. Caselli, M. Wolf, P. Baglionia, D. Berti, Nanoscale 10 (2018) 3480–3488.
[49] I. Zawisza, X. Bin, J. Lipkowski, Langmuir 23 (2007) 5180–5194.
[50] H. Binder, Appl. Spectrosc. Rev. 38 (2003) 15–69.
[51] Z. Liu, D. Wang, M. Cao, Y. Han, H. Xu, Y. Wang, ACS Appl. Mater. Interfaces 7 (2015) 15078–15087.
[52] M.S. Islam, S.M. Shortall, G.M. Mekhail, S.P. Callender, O. Madkhali, Z. Bharwani, D. Ayyash, K. Kobernyk, S.D. Wettig, Phys. Chem. Chem. Phys. 19 (2017) 10825–10834.
[53] I.C.M. Kwan, Y.-M. She, G. Wu, Can. J. Chem. 89 (2011) 835–844.
[54] L. Xu, M. Chen, J. Hao, J. Phys. Chem. B 121 (2017) 420–425.
[55] F. Morale, R.W. Date, D. Guillon, D.W. Bruce, R.L. Finn, C. Wilson, A.J. Blake, M. Schröder, B. Donnio, Chem. Eur. J. 9 (2003) 2484–2501.
[56] S. Laschat, A. Baro, N. Steinke, F. Giesselmann, C. Hägele, G. Scalia, R. Judele, E. Kapatsina, S. Sauer, A. Schreivogel, M. Tosoni, Angew. Chem. Int. Ed. 46 (2007) 4832–4887.
[57] M.M. Neidhardt, M. Wolfrum, S. Beardsworth, T. Wöhrle, W. Frey, A. Baro, C. Stubenrauch, F. Giesselmann, S. Laschat, Chem. Eur. J. 22 (2016) 16494–16504.
[58] N. Godbert, A. Crispini, M. Ghedini, M. Carini, F. Chiaravalloti, A. Ferrise, J. Appl. Crystallogr. 47 (2014) 668–679.
[59] T. Kobayashi, T. Ichikawa, T. Kato, H. Ohno, Adv. Mater. 29 (2017) 1604429.
[60] K. Liu, M. Shuai, D. Chen, M. Tuchband, J.Y. Gerasimov, J. Su, Q. Liu, W. Zajaczkowski, W. Pisula, K. Müllen, N.A. Clark, A. Herrmann, Chem. Eur. J. 21 (2015) 4898–4903.
[61] H. Zheng, C.K. Lai, T.M. Swager, Chem. Mater. 7 (1995) 2067–2077.
[62] L. Wang, S. Dong, J. Hao, Curr. Opin. Colloid Interface Sci. 35 (2018) 81–90.
[63] A. Immirzi, B. Perini, Acta Cryst. Sect. A 33 (1977) 216–218.
[64] M. Panda, J.A. Walmsley, J. Phys. Chem. B 115 (2011) 6377–6383.
[65] J. Kim, S. Cho, B.K. Cho, Chem. Eur. J. 20 (2014) 12734–12739.